PARTICULATE SCIENCE AND TECHNOLOGY
2019, VOL. 37, NO. 5, 616–622
https://doi.org/10.1080/02726351.2017.1414091

Taylor & Francis
Taylor & Francis Group

RF plasma modified W_5O_{14} and MoS_2 hybrid nanostructures and photovoltaic properties

Sule Erten Ela[a], Maja Remskar[b], Gozde Yurdabak Karaca[c], Lutfi Oksuz[d], Emre Uygun[d], and Aysegul Uygun Oksuz[c]

[a]Solar Energy Institute, Ege University, İzmir, Turkey; [b]Solid State Physics Department, Jozef Stefan Institute, Ljubljana, Slovenia; [c]Faculty of Arts and Science, Department of Chemistry, Suleyman Demirel University, Isparta, Turkey; [d]Faculty of Arts and Science, Department of Physics, Suleyman Demirel University, Isparta, Turkey

ABSTRACT

Modification of W_5O_{14} and MoS_2 nanostructures was carried out using 3,4-ethylenedioxythiophene monomer in a capacitively coupled, RF rotating plasma reactor. Raman spectroscopy and X-ray diffraction (XRD) measurements were used for structural characterization. The surface morphologies of nanomaterials were investigated using transmission electron microscopy. Polymer coated (W_5O_{14}/PEDOT, MoS_2/PEDOT) and untreated (W_5O_{14}, MoS_2) nanostructures were used as the counter electrode for dye-sensitized solar cells. Photovoltaic performances of W_5O_{14}/PEDOT and MoS_2/PEDOT hybrid nanostructures were higher than those of W_5O_{14} and MoS_2 inorganic nanostructures. Our results indicate that plasma polymer coated W_5O_{14} and MoS_2 nanostructures of the device for cathode increase both its fill factor and its energy conversion efficiency.

KEYWORDS

Counter electrode; hybrid; MoS_2; RF rotating plasma; W_5O_{14}

1. Introduction

Nanosized materials have been widely used in many applications due to their size-dependent and low-dimensional physical and chemical properties, different from those of the bulk materials (Remskar et al. 2007; Lin et al. 2011). Due to the unique properties, including optical, gas-sensing, electrochromic, and field emission properties, tungsten oxide nanoparticles have been widely investigated (Su et al. 2010). Several substoichiometric structures of WO_x ($2.625 \leq x \leq 2.92$) have been experimentally observed like tetragonal W_5O_{14} (Migas et al. 2010). They are known as Magneli phases, homologous series of transition metal suboxides with unusual composition (Remskar et al. 2007). Among the various tungsten oxide phases, non-stoichiometric W_5O_{14} particularly exhibits highly favorable properties as compared WO_3 (Su et al. 2009). Recently, research on nanomaterials with their size-dependent and low-dimensional physical and chemical properties recalled the scientific attention to tungsten suboxides, which show high aspect ratios and promising physical properties on the nanoscale. Nanomaterials as compared to the corresponding bulk compounds show greatly enhanced gas-sensing performance and improved photochromic effects. W_5O_{14} nanowires, which was confirmed also with direct transport measurements on a double-stranded nanowire, which is important for their use in nanoelectronics (Remskar et al. 2007).

MoS_2 is one of the important layered transition metal chalcogenides. The ultralow friction and wear properties of MoS_2 fullerene like particles make inorganic fullerenes important tribological materials (Remskar et al. 2001). MoS_2 nanoparticles have important applications as solid lubricants, photovoltaic films, catalyst, absorbers, etc. (Hoshyargar et al. 2011).

The polymerization process of materials has been mainly realized by solution-based wet methods such as chemical and electrochemical (Guimard, Gomez, and Schmidt 2007; Oksuz et al. 2013). The disadvantages of wet processing method are low reproducibility, large chemical consumption, multiple steps, and long processing time. In contrast, plasma polymerization method is a dry process, a solvent-free, nontoxic, and single-step process (Guimard, Gomez, and Schmidt 2007). Moreover, the plasma polymerization process has advantage of rapid deposition of thin polymer layers on to the nanotubes and nanowires. Among the plasma polymerization process, radio frequency (RF) rotating plasma coating system provides homogeneous coatings on to the surface and with a variety of thickness. Recently, RF rotating plasma has been used to obtain homogenously hybrid powders. Our group successfully obtained the hybrid systems under RF rotating plasma conditions. The modification of multi-walled carbon nanotube with poly(3-hexylthiophene) and polypyrrole (PPy) was indicated the homogenously and controlling coatings and better properties using fast, versatile, and environmentally friendly RF rotating plasma process (Cogal et al. 2016). Kiristi et al. coated poly(3,4-ethylenedioxythiophene) (PEDOT) onto WO_3 powders by RF rotating plasma and obtained good stability and coloration efficiency for hybrid ECD on glass substrate (Kiristi et al. 2014). Our group also were modified, V_2O_5 powders with PEDOT using RF rotating plasma system for electrochromic device applications (Karaca et al. 2017). The advantages of RF rotating plasma conditions, free radicals, and ions of

CONTACT Aysegul Uygun Oksuz ayseguluygun@sdu.edu.tr Faculty of Arts and Science, Department of Chemistry, Suleyman Demirel University, Isparta 32260, Turkey.
Color versions of one or more of the figures in the article can be found online at www.tandfonline.com/upst.

monomers are obtained and recombination of these radicals and ions has formed high conjugated plasma polymers (Cogal et al. 2016).

In this study, W_5O_{14} nanowires and MoS_2 nanotubes were coated homogeneously with PEDOT using RF rotating plasma polymerization method. As a further step, the cathode electrode properties of the modified materials were compared for dye-sensitized solar cells (DSSCs) applications.

Conventional DSSCs undergo stability problems that result from their use of liquid electrolytes along with platinum counter electrode, which causes electrolyte leakage and electrode corrosion. Still, the expensive fabrication of DSSCs using a platinum catalyst is hindered by its insufficient scarcity and high cost (Malara et al. 2011). Tungsten and molybdenum oxides are good selections for counter electrode in DSSCs because of high electrocatalytic activity. Conjugated polymers, such as PPy, polyaniline, poly(3,4-propylenedioxythiophene), PEDOT have attracted much interest as alternative CEs in DSSCs due to the ambient temperatures used in their synthesis as well as conducting nature and facile deposition methods (Qin et al. 2011; Thomas et al. 2014; Yun et al. 2015). Recently, organic hole-transporting materials such as PEDOT have been successfully applied for the construction of solid-state DSSCs due to their strong ability of hole transport and storage (Melas-Kyriazi et al. 2011; Zhang et al. 2011; Liu et al. 2012).

2. Experimental

2.1. Synthesis of W_5O_{14} nanowires and MoS_2 nanotubes

W_5O_{14} nanowires were synthesized by chemical transport reaction using WO_3 as source of tungsten and metallic nickel as growth promoter. The materials were transported from 1133 to 1009 K under 6.2°C/cm temperature gradient. Transport reaction runs for 500 h. The W_5O_{14} nanowires of bright blue color were up to several millimeters long with diameters around 100 nm.

MoS_2 nanotubes were prepared by sulfurization of Mo_6S_{2I8} nanowires (Nanotul Ltd.) in H_2S (1%)/H_2 (1%)/argon (98%) flowing gas at 1073 K. The reaction runs for 2 h. The product composed of pure MoS_2 nanotube which kept outer shape of the starting material. The nanotubes were up to 5 μm in length and around 100 nm in diameter.

2.2. Plasma PEDOT polymerization of MoS_2 nanotube and W_5O_{14} nanowire

The uniform polymerization of 3,4-ethylenedioxythiophene (EDOT)-based polymer PEDOT onto W_5O_{14} nanowires and MoS_2 nanotubes was carried out in a capacitively coupled, 13.56 MHz RF rotating plasma reactor. Steady-state plasma polymerization conditions were applied for both modifications during 30 min and the working pressure of 50 mTorr. To modify nanotubes and nanowires, EDOT monomer was sent to the rotating chamber and plasma was created through 30 Watt. This plasma polymerization technique has the advantage of homogeneous outer surface coating because of the rotation of the glass reactor vacuum chamber. The mechanism of plasma polymerization is attributed to the collisions of the monomer molecules with the electrons generated by the electric discharges, and such reactions are a major source of free radicals of EDOT monomer and negative ions of structure (Wang et al. 2002; Karaca et al. 2017). Plasma polymerization process is shown in Figure 1. The RF rotating plasma setup is shown in Figure 2.

2.3. Characterization

X-ray diffraction analyses were performed using Siemens D-5000 with CuKα radiation (λ: 1.54 Å). The diffraction data were recorded for 2θ angles between 20° and 60°. Transmission electron microscopy (TEM) images were taken on a model HR-TEM Jeol 2010 F, field emission model TEM analysis model. The Raman spectra were obtained using a WITec CRM200 Raman system with 1800 and 150 lines/mm grating, respectively, with 532 nm excitation laser. Gamry PCl4/300 model potentiostat was used for electrochemical studies. Electrochemical experiments were carried out using conventional three-electrode cell, a working electrode, a Pt wire counter, and an Ag/AgCl with 3 M KCl reference electrodes.

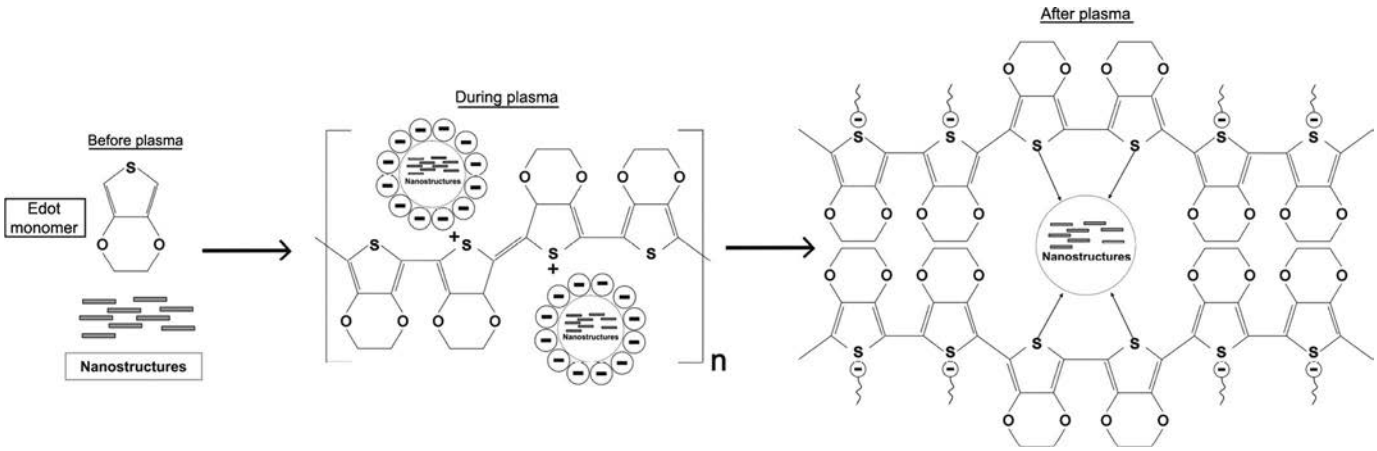

Figure 1. Plasma polymerization process.

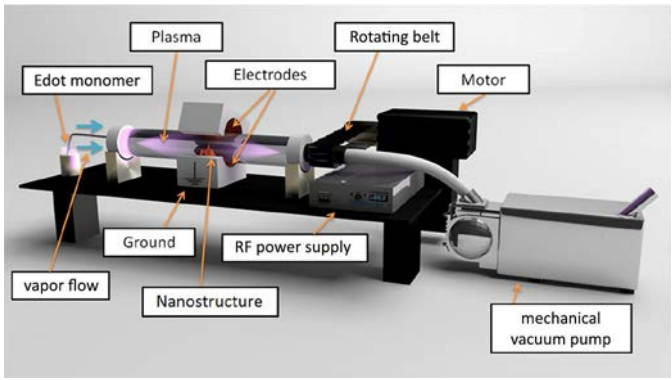

Figure 2. RF Rotating plasma setup.

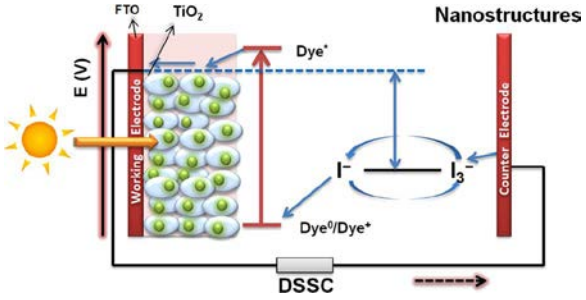

Figure 3. Schematic diagram of fabricated dye-sensitized solar cell (DSSC).

2.4. Fabrication of DSSCs

The TiO_2 electrodes were heated to 450°C for 20 min in an ambient atmosphere and left to cool to 80°C prior to immersing into an ethanol solution containing dye (0.5 mM) overnight. The cells were fabricated using MoS_2, MoS_2/PEDOT, W_5O_{14}, and W_5O_{14}/PEDOT CEs.

And then, cells sealed with a 30 µm Surlyn (Dupont) by resistive heating. Electrolyte solution (0.6 M *N*-methyl-*N*-butyl-imidazolium iodide (BMII) + 0.1 M LiI +0.05 M I_2 + 0.5 M 4-tert-butylpyridine in acetonitrile) was injected via vacuum backfilling through a hole in the counter electrode and the hole was covered with bynel. Figure 3 shows the schematic diagram of fabricated DSSC.

2.5. DSSC measurements

Dye-sensitized solar cells were recorded a Newport oriel solar simulator equipped with a class A 150 W xenon light source for current–voltage measurement. The power output of the lamp was measured to one sun. All current–voltage characteristics were done under 100 mW/cm^2 light intensity and AM 1.5 conditions. All cells were measured with a mask size of 0.16 cm^2. 450 W Xenon light source (Oriel) was used to give an irradiance of various intensities. J−V measurements were carried out using Keithley 2400 Source-Meter system and LabView data acquisition software.

3. Results and discussion

3.1. XRD results

Figure 4 shows the XRD spectra of W_5O_{14} nanowires (a) and of the W_5O_{14}/PEDOT nanocomposite (b). Both spectra are

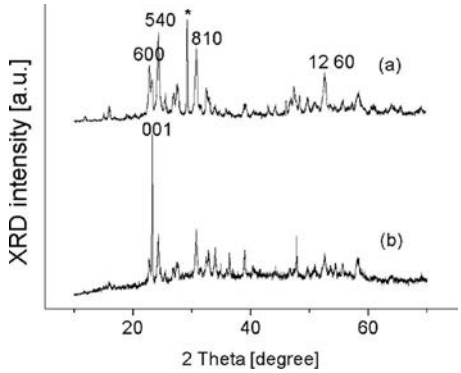

Figure 4. XRD spectrum: (a) W_5O_{14}; (b) W_5O_{14}/PEDOT. *Note*: PEDOT, poly(3,4-ethylenedioxythiophene); XRD, X-ray diffraction.

attributed to W_5O_{14} and assigned according to JCPDS-71-0292. A relatively low (001) peak in the spectrum, which is in bulk W4O14 the most intensive, is explained by the geometry where majority of the nanowires, which are grown along [001] direction, lay flat on the plastelin used for the sample fixing onto the XRD holder. A peak at 29.2° belongs to the plastelin (labeled with*). Therefore, majority of the nanowires, which growing along (001) direction, were parallel with the substrate, and the spectrum of W_5O_{14} nanowires (Figure 4a) shows relatively strong (hk0) peaks. The peak labeled with corresponds to the used clay. The nanowires covered by PEDOT were oriented randomly. Their XRD spectrum (Figure 4b) reveals the strongest (hk1) peaks and suppressed (hk0) peaks. There is no additional peak visible besides W_5O_{14}.

Figure 5 shows XRD spectra of MoS_2 nanotubes (a) and MoS_2/PEDOT nanocomposite. They are practically identical with the only difference in slightly smaller (002) peak in MoS_2/PEDOT, which is also caused by more random oriented nanotubes in the nanocomposite with respect to powder like MoS_2 sample.

3.2. TEM results

The W_5O_{14} nanowires are rigid with length up to several millimeters and diameters around 100 nm (Figure 6a). After PEDOT deposition, they were covered with PEDOT layer with thickness which varying from 1 nm to 5 nm (Figure 6b). The

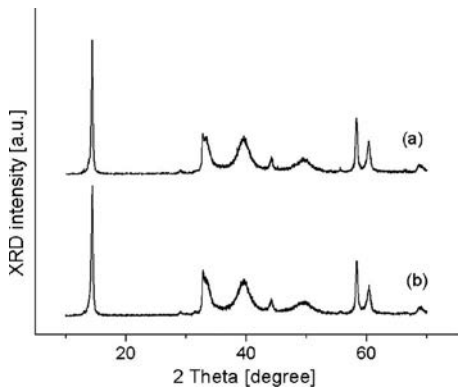

Figure 5. XRD spectrum: (a) MoS_2; (b) MoS_2/PEDOT. *Note*: PEDOT, poly(3,4-ethylenedioxythiophene); XRD, X-ray diffraction.

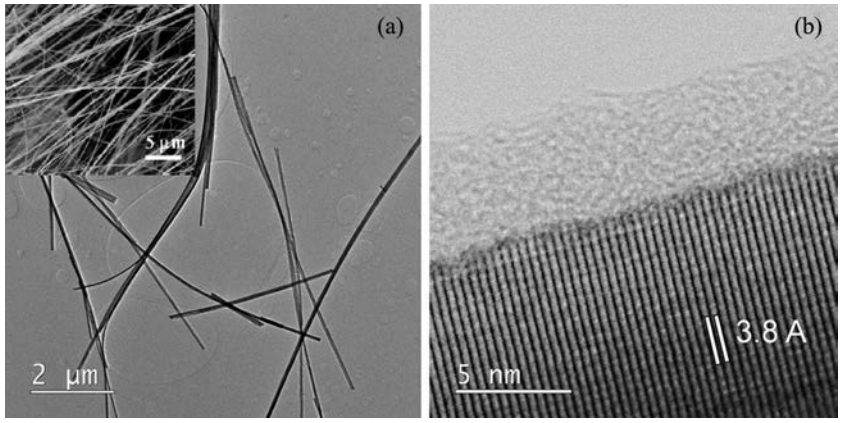

Figure 6. High-resolution TEM images: (a) rigid W_5O_{14} nanowires with a high aspect ratio; (b) high-resolution image of an edge of W_5O_{14} crystal covered with 4.5 nm of amorphous PEDOT. Stripes oriented perpendicular to the nanowire's axis is 3.8 Å apart. *Note*: PEDOT, poly(3,4-ethylenedioxythiophene); TEM, transmission electron microscopy.

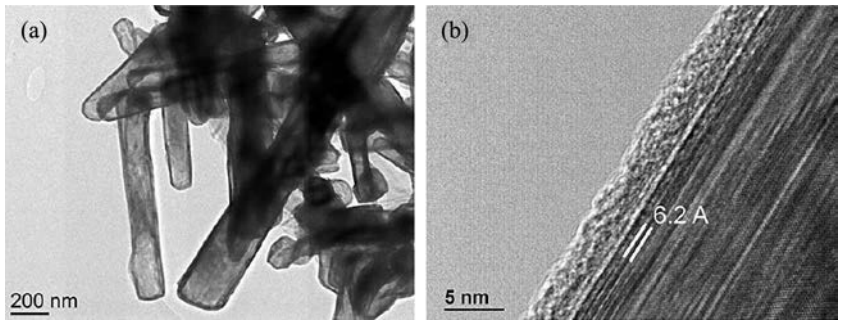

Figure 7. High-resolution TEM images: (a) MoS_2 nanotubes with length up to 5 μm, diameter up to 200 nm and wall thickness around 10 nm; (b) 3 nm thick amorphous PEDOT coating on a MoS_2 nanotube. *Note*: TEM, transmission electron microscopy.

nanowires grow along a-axis of the crystals of tetragonal symmetry and lattice parameters: $a = 23.33(1)$ Å and $c = .797(1)$ Å (JCPDS 71-0292, reference McColm). The distance between fringes oriented in Figure 6b, which are oriented perpendicular to the nanowire's axis, is in a good agreement with the (001) interplanar distance (3.7970 Å) of W_5O_{14}.

The MoS_2 nanotubes grow with relatively small aspect ratio 1:50 (Figure 7a) in comparison with W_5O_{14} nanowires. The nanotube dome is closed with wall thickness around 10 nm. They are self-assembled into weakly bonded agglomerates. Thickness of PEDOT coating was around 3 nm in average, but it varied from a place to place due to spontaneous disassembly of the agglomerates during sample manipulation (Figure 7b). The freshly disassembled nanotubes were without PEDOT coating, while those which have been exposed to PEDOT deposition is coated with relatively homogeneous polymer layer.

3.3. Raman spectroscopy results

Raman spectra of W_5O_{14} nanowires and of W_5O_{14} nanowires covered by PEDOT are shown in Figure 8. Overall characteristics of the Raman spectra were not changed by deposition of PEDOT although two peaks were slightly shifted. Positions of the main Raman bands in W_5O_{14} are at 134, 260, 707, and 809 cm^{-1} while the positions are at 134, 265, 715, and 809 cm^{-1} for in the W_5O_{14}/PEDOT. The two downshifted peaks (260 cm^{-1}, 707 cm^{-1}), which could originate from O-W-O bending mode and W-O stretching mode assuming crystal structure similarity with $W_{18}O_{49}$ (Guo et al. 2012; Li et al. 2014), are

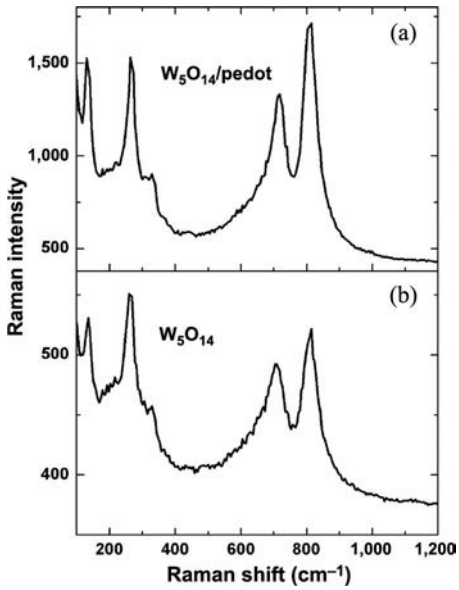

Figure 8. Raman spectra: (a) W_5O_{14} nanowires; (b) W_5O_{14} nanowires with PEDOT coating. *Note*: PEDOT, poly(3,4-ethylenedioxythiophene).

explained by thermal effect in pure W_5O_{14} sample (Lu et al. 2007). Local heating of the W_5O_{14}/PEDOT is obviously smaller because the Raman bands are not shifted. The reason could be better thermal contact through PEDOT with Si wafer used as a substrate.

Figure 9 shows Raman spectra of (a) MoS_2 NTs and (b) MoS_2/PEDOT composite. Both spectra reveal a strong indication of partial oxidation of MoS_2 NTs to α -MoO_3. The main peaks originated from the remained MoS_2 are at the positions: 386 and 411 cm^{-1} (MoS_2 NTs) and at 383 and 409 cm^{-1} (MoS_2 NTs/PEDOT). While the Raman peaks recorded in MoS_2/PEDOT are in relatively good agreement with literature for MoS_2 (383 cm^{-1}, 408 cm^{-1}) (Viršek et al. 2010; Li et al. 2012), a blue shift of these peaks for 3 cm^{-1} and 2 cm^{-1}, respectively, was found in MoS_2 NTs. This blue shift could be explained by partial oxidation of the MoS_2 which took place in larger extend than in MoS_2/PEDOT. Indeed, in both spectra, a strong contribution of α -MoO_3 is visible with the main peaks at 826 and 1000 cm^{-1}, and some weaker peaks of the same origin at 237, 337, 290, and 670 cm^{-1}. Due to very thin walls of the NTs in a range of 10 nm, and preserved cylindrical geometry, their partial oxidation could lead to a stiffer structure. Like in a case of W_5O_{14}, PEDOT coating increased thermal conductance and decreased annealing of MoS_2 NTs which were less prone to oxidation after coating.

3.4. Electrochemical results (CAs)

To get a deeper insight into their electroactivity and stability, the electrochemical behavior of the nanostructures was studied by chronoamperometry (CA) in 1 M $LiClO_4$/ACN solution. Gamry PCl4/300 model potentiostat was used for electrochemical studies. CA measurements of W_5O_{14}, W_5O_{14}/PEDOT, MoS_2, and MoS_2/PEDOT were carried out in a three-electrode electrochemical cell with nanostructures were dropped onto the Pt disc electrode used as working electrode, Ag/AgCl/3 M KCl reference electrode, and a Pt wire as counter electrode at a scan rate of 100 mV/s during 60 seconds. CA in Figure 10 suggests that they exhibit good electroactivity within both W_5O_{14} and W_5O_{14}, MoS_2 and MoS_2/PEDOT ±2 V potential range was studied. Cathodic current wave is the result of application of − 2V and anodic current wave is due to the application of + 2V between working electrode and counter electrode for 30 s. Figure 10a and b bear out the fact that the W_5O_{14}, W_5O_{14}/PEDOT and MoS_2, MoS_2/PEDOT were exhibited reversible and stable electroactivity property. Both modified nanostructures (MoS_2/PEDOT, W_5O_{14}/PEDOT) have higher current density compared with untreated ones (MoS_2 and W_5O_{14}) (Table 1).

3.5. DSSC measurements

Photovoltaic performances of DSSCs were investigated using MoS_2, MoS_2/PEDOT, W_5O_{14}, W_5O_{14}/PEDOT counter electrodes. Figure 11 shows the current density–voltage (J-V) curves of DSSCs using MoS_2, MoS_2/PEDOT, W_5O_{14}, and W_5O_{14}/PEDOT CEs.

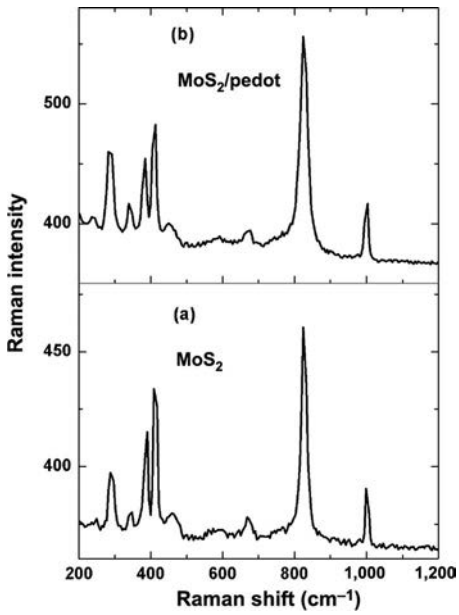

Figure 9. Raman spectra; (a) MoS_2 nanotubes; (b) MoS_2 nanotubes with PEDOT coating. *Note*: PEDOT, poly(3,4-ethylenedioxythiophene).

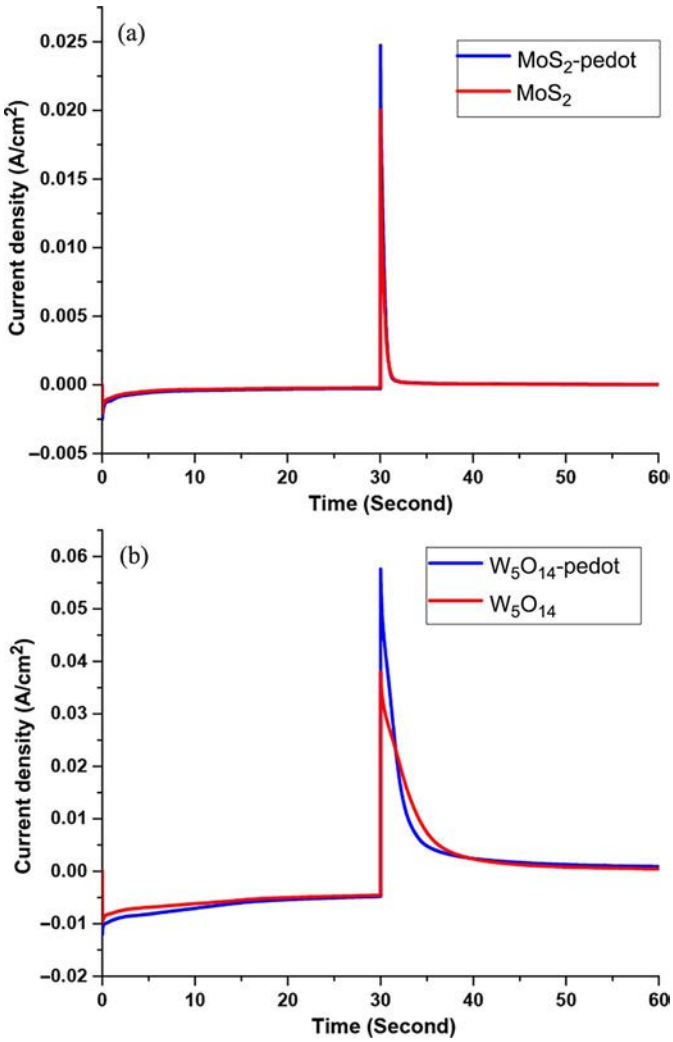

Figure 10. Chronoamperometric response of the a) MoS_2/PEDOT, MoS_2 b) W_5O_{14}/PEDOT, W_5O_{14}. *Note*: PEDOT, poly(3,4-ethylenedioxythiophene).

Table 1. Current densities of the nanostructures according to chronoamperometric results.

Nanostructure	Current density (A/cm^2)
MoS_2	0.020
MoS_2-PEDOT	0.025
W_5O_{14}	0.038
W_5O_{14}-PEDOT	0.058

PEDOT, poly(3,4-ethylenedioxythiophene).

Table 2. Photovoltaic parameters of MoS_2, MoS_2/PEDOT, W_5O_{14}, W_5O_{14}/PEDOT using as counter electrodes.

	J_{sc} (mA cm^{-2})	V_{oc} (mV)	FF	η (%)
MoS_2	3.21	350	0.12	0.13
MoS_2-PEDOT	5.61	350	0.16	0.30
W_5O_{14}	5.75	500	0.11	0.32
W_5O_{14}-PEDOT	13.10	500	0.22	1.44

PEDOT, poly(3,4-ethylenedioxythiophene).

Power conversion efficiency (PCE) is calculated as (Wang and Lin 2010);

PCE $= \frac{J_{SC}V_{OC}FF}{P_{inc}}$, where J_{sc} is the short circuit current density, V_{oc} is the open-circuit voltage, FF is the fill factor, and P_{inc} is 100 mW/cm^2 light intensity in all current–voltage characteristics.

In Table 2, DSSCs using W_5O_{14}/PEDOT CE give high short circuit current density (J_{sc}) of 13.10 mAcm^{-2}, a fill factor (FF) of 0.22, an open-circuit voltage (V_{oc}) of 500 mV, and PCE of 1.44%. In contrast, photovoltaic parameters of DSSC using MoS_2/PEDOT CE exhibit a short circuit current density (J_{sc}) of 5.61 mAcm^{-2}, a fill factor (FF) of 0.16, an open-circuit voltage (V_{oc}) of 350 mV, and PCE of 0.30%. As compared with DSSC, using W_5O_{14}/PEDOT and MoS_2/PEDOT is improved from 5.61 to 13.10 mAcm^{-2}, FF is improved from 0.16 to 0.22, which surpasses the PCE of DSSC from 0.30 to 1.44%. A solar cell can effectively utilize the photonic energy and optimize open-circuit voltage, which leads to high PCE with adopting polymer (Chen et al. 2009; You et al. 2013). Both W_5O_{14}/PEDOT and MoS_2/PEDOT FF values improvement compared with untreated ones can be related to the decrease in the series resistance of the device that results from the insertion of a PEDOT layer (Song, Kim, et al. 2004). The good photovoltaic performance of DSSC using MoS2/PEDOT-PSS counter electrode is primarily derived from the high electrocatalytic activity of nanosized MoS_2 and the high conductive feature of PEDOT-PSS (Song, Li, et al. 2014). In another study, treated WO_3 nanomaterials, which conductivity increase with doped materials, were used as counter electrode and it is comparable to that of DSSC using standard Pt counter electrode

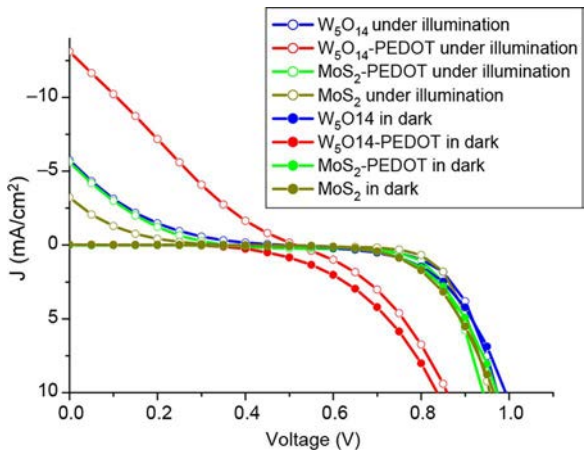

Figure 11. J–V curve of DSSC using MoS_2, MoS_2/PEDOT, W_5O_{14}, W_5O_{14}/PEDOT counter electrodes. *Note*: DSSC, dye-sensitized solar cell; PEDOT, poly(3,4-ethylenedioxythiophene).

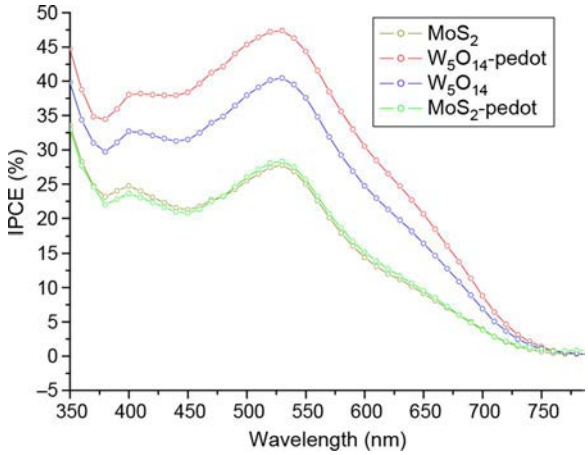

Figure 12. IPCE curve of DSSC using MoS_2, MoS_2/PEDOT, W_5O_{14}, W_5O_{14}/PEDOT counter electrodes. *Note*: DSSC, dye-sensitized solar cell; PEDOT, poly(3,4-ethylenedioxythiophene).

(Song et al. 2016). The hybrid nanostructures obtained by RF rotating plasma are less conductive than the hybrid nanostructures obtained by chemical or electrochemical method (Cogal et al. 2016). In our results, both W_5O_{14}/PEDOT and MoS_2/PEDOT counter electrodes indicated better FF values those of W_5O_{14} and MoS_2 counter electrodes.

The improvement in the PCE (Figure 12) of DSSCs can be attributed to the high performance of W_5O_{14}-PEDOT which (as the chronoamperometric response experiments confirm) possesses a combination of high catalytic activity and good electrical conductivity.

4. Conclusion

The nanostructures were homogeneously modified using RF rotating plasma technique. Polymer-modified (W_5O_{14}/PEDOT, MoS_2/PEDOT) nanostructures used as the counter electrode for dye-sensitized solar cells (DSSCs) leads to high PCE. Especially, W_5O_{14}/PEDOT has more efficiency compared with MoS_2/PEDOT used as counter electrode. This result is justified with chronoamperometric results which showed W_5O_{14}/PEDOT has good stability. Also, DSSC results showed that W_5O_{14}/PEDOT has effective photovoltaic properties than other nanostructures. This polymerization of the device for cathode increases both its fill factor and its energy conversion efficiency.

Funding

Authors gratefully acknowledge the TUBITAK COST (Project No: 213M562) to support this study.

References

Chen, H.-Y., J. Hou, S. Zhang, Y. Liang, G. Yang, Y. Yang, L. Yu, Y. Wu, and G. Li. 2009. Polymer solar cells with enhanced open-Circuit voltage and efficiency. *Nature Photonics* 3 (11):649–53. doi:10.1038/nphoton.2009.192.

Cogal, S., S. E. Ela, G. C. Cogal, M. Micusik, M. Omastova, and A. U. Oksuz. 2016. Plasma-enhanced modification of multiwalled carbon nanotube with conducting polymers for dye sensitized solar cells. *Polymer Composites*. doi:10.1002/pc.23983.

Guimard, N. K., N. Gomez, and C. E. Schmidt. 2007. Conducting polymers in biomedical engineering. *Progress in Polymer Science* 32 (8–9):876–921. doi:10.1016/j.progpolymsci.2007.05.012.

Guo, C., S. Yin, M. Yan, M. Kobayashi, M. Kakihana, and T. Sato. 2012. Morphology-controlled synthesis of $W_{18}O_{49}$ nanostructures and their near-infrared absorption properties. *Inorganic Chemistry* 51 (8):4763–71. doi:10.1021/ic300049j.

Hoshyargar, F., A. Yella, M. Panthöfer, and W. Tremel. 2011. Diffusion-driven formation of MoS_2 nanotube bundles containing MoS_2 nanopods. *Chemistry of Materials* 23 (21):4716–20. doi:10.1021/cm201460z.

Karaca Y., E. E. Gozde, C. Alver, U. Koc, E. Uygun, L. Oksuz, and A. U. Oksuz. 2017. Plasma modified V_2O_5/PEDOT hybrid based flexible electrochromic devices. *Electroanalysis* 29 (5):1324–31. doi:10.1002/elan.201600631.

Kiristi, M., F. Bozduman, A. U. Oksuz, L. Oksuz, and A. Hala. 2014. Solid state electrochromic devices of plasma modified WO3 hybrids. *Industrial & Engineering Chemistry Research* 53 (41):15917–22. doi:10.1021/ie5025613.

Li, F., H. Gong, Y. Wang, H. Zhang, Y. Wang, S. Liu, S. Wang, and C. Sun. 2014. Enhanced activity, durability and anti-poisoning property of Pt/$W_{18}O_{49}$ for methanol oxidation with a sub-Stoichiometric tungsten oxide $W_{18}O_{49}$ support. *Journal of Materials Chemistry A* 2 (47):20154–63. doi:10.1039/c4ta04220d.

Li, H., Q. Zhang, C. C. R. Yap, B. K. Tay, T. H. T. Edwin, A. Olivier, and D. Baillargeat. 2012. From bulk to monolayer MoS_2: Evolution of Raman scattering. *Advanced Functional Materials* 22 (7):1385–90. doi:10.1002/adfm.201102111.

Lin, H.-C., C.-Y. Su, Z.-K. Yang, C.-K. Lin, and K.-L. Ou. 2011. A facile route to tungsten oxide nanomaterials with controlled morphology and structure. *Particuology* 9 (5):517–21. doi:10.1016/j.partic.2011.01.006.

Liu, P., H. X. Yang, X. P. Ai, G. R. Li, and X. P. Gao. 2012. A solar rechargeable battery based on polymeric charge storage electrodes. *Electrochemistry Communications* 16 (1):69–72. doi:10.1016/j.elecom.2011.11.035.

Lu, D. Y., J. Chen, J. Zhou, S. Z. Deng, N. S. Xu, and J. B. Xu. 2007. Raman spectroscopic study of oxidation and phase transition in $W_{18}O_{49}$ nanowires. *Journal of Raman Spectroscopy* 38 (2):176–80. doi:10.1002/jrs.1620.

Malara, F., M. Manca, L. De Marco, P. Pareo, and G. Gigli. 2011. Flexible carbon nanotube-based composite plates as efficient monolithic counter electrodes for dye solar cells. *ACS Applied Materials & Interfaces* 3 (9):3625–32. doi:10.1021/am200838q.

Melas-Kyriazi, J., I.-K. Ding, A. Marchioro, A. Punzi, B. E. Hardin, G. F. Burkhard, N. Tétreault, M. Grätzel, J.-E. Moser, and M. D. Mcgehee. 2011. The effect of hole transport material pore filling on photovoltaic performance in solid-state dye-sensitized solar cells. *Advanced Energy Materials* 1 (3):407–14. doi:10.1002/aenm.201100046.

Migas, D. B., V. L. Shaposhnikov, and V. E. Borisenko. 2010. Tungsten oxides. II. The metallic nature of Magnéli phases. *Journal of Applied Physics* 108 (9):093714. doi:10.1063/1.3505689.

Oksuz, A. U., S. Manolache, L. Oksuz, and N. Hershkowitz. 2013. Plasma Nanocoating of Thiophene onto TiO_2 Nanoparticles. *Industrial & Engineering Chemistry Research* 52 (19):6610–16. doi:10.1021/ie303176j.

Qin, Q., J. Tao, Y. Yang, and X. Dong. 2011. In situ oxidative polymerization of polyaniline counter electrode on ITO conductive glass substrate. *Polymer Engineering & Science* 51 (4):663–69. doi:10.1002/pen.21858.

Remskar, M., J. Kovac, M. Viršek, M. Mrak, A. Jesih, and A. Seabaugh. 2007. W_5O_{14} nanowires. *Advanced Functional Materials* 17 (12):1974–78. doi:10.1002/adfm.200601150.

Remskar, M., A. Mrzel, Z. Skraba, A. Jesih, M. Ceh, J. Demsar, P. Stadelmann, F. Levy, and D. Mihailovic. 2001. Self-assembly of subnanometer-diameter single-wall MoS_2 nanotubes." *Science* 292 (5516):479–81. doi:10.1126/science.1059011.

Song, D., Z. Chen, P. Cui, M. Li, X. Zhao, Y. Li, and L. Chu. 2016. NH_3-treated WO3 as low-cost and efficient counter electrode for dye-sensitized solar cells. *Nano Online* 10. doi:10.1515/nano.11671_2014.8.

Song, D., M. Li, Y. Jiang, Z. Chen, F. Bai, Y. Li, and B. Jiang. 2014. Facile fabrication of MoS_2/PEDOT–PSS composites as low-cost and efficient counter electrodes for dye-sensitized solar cells. *Journal of Photochemistry and Photobiology A: Chemistry* 279:47–51. doi:10.1016/j.jphotochem.2014.01.009.

Song, M. Y., D. K. Kim, K. J. Ihn, S. M. Jo, and D. Y. Kim. 2004. Electrospun TiO_2 electrodes for dye-sensitized solar cells. *Nanotechnology* 15 (12):1861–65. doi:10.1088/0957-4484.15.12.030.

Su, C.-Y., H.-C. Lin, T.-K. Yang, C.-H. Chang, and C.-K. Lin. 2009. Tungsten oxide nanopowders and nanorods prepared by a modified plasma arc gas condensation technique. *Materials Transactions* 50 (11):2593–97. doi:10.2320/matertrans.m2009068.

Su, C.-Y., H.-C. Lin, T.-K. Yang, and C.-K. Lin. 2010. The effect of processing parameters on the synthesis of tungsten oxide nanomaterials by a modified plasma arc gas condensation technique." *Journal of Nanoscience and Nanotechnology* 10 (8):5461–66. doi:10.1166/jnn.2010.1946.

Thomas, S., T. G. Deepak, G. S. Anjusree, T. A. Arun, S. V. Naira, and A. S. Nair. 2014. A review on counter electrode materials in dye-sensitized solar cells. *J. Mater. Chem. A* 2:4474–90. doi:10.1039/C3TA13374E.

Viršek, M., M. Krause, A. Kolitsch, A. Mrzel, I. Iskra, S. D. Škapin, and M. Remškar. 2010. The transformation pathways of $Mo_6S_2I_8$ nanowires into morphology-selective MoS_2 nanostructures. *J. Phys. Chem. C* 114 (14):6458–63. doi:10.1021/jp101298g.

Wang, J., and Z. Lin. 2010. Dye-sensitized TiO_2 nanotube solar cells with markedly enhanced performance via rational surface engineering. *Chemistry of Materials* 22 (2):579–84. doi:10.1021/cm903164k.

Wang, J., K. G. Neoh, L. Zhao, and E. T. Kang. 2002. Plasma polymerization of aniline on different surface functionalized substrates. *Journal of Colloid and Interface Science* 251 (1):214–24. doi:10.1006/jcis.2002.8389.

You, J., L. Dou, K. Yoshimura, T. Kato, K. Ohya, T. Moriarty, K. Emery et al. 2013. A polymer tandem solar cell with 10.6% power conversion efficiency. *Nature Communications* 4 (May):1446. doi:10.1038/ncomms2411.

Yun, S., Y. Liu, T. Zhang, and S. Ahmad. 2015. Recent advances in alternative counter electrode materials for co-mediated dye-sensitized solar cells. *Nanoscale* 7 (28):11877–93. doi:10.1039/c5nr02433a.

Zhang, W., Y. Cheng, X. Yin, and B. Liu. 2011. Solid-state dye-sensitized solar cells with conjugated polymers as hole-transporting materials. *Macromolecular Chemistry and Physics* 212 (1):15–23. doi:10.1002/macp.201000489.